Astrophys Space Sci (2007) 308: 279–286
DOI 10.1007/s10509-007-9366-2

ORIGINAL ARTICLE

Thin magnetic hydrogen atmospheres and the neutron star RX J1856.5–3754

Wynn C.G. Ho · David L. Kaplan · Philip Chang · Matthew van Adelsberg · Alexander Y. Potekhin

Received: 1 July 2006 / Accepted: 31 August 2006 / Published online: 21 March 2007

Abstract RX J1856.5–3754 is one of the brightest nearby isolated neutron stars, and considerable observational resources have been devoted to it. However, current models are unable to satisfactorily explain the data. We show that our latest models of a thin, magnetic, partially ionized hydrogen atmosphere on top of a condensed surface can fit the entire spectrum, from X-rays to optical, of RX J1856.5–3754, within the uncertainties. In our simplest model, the best-fit parameters are an interstellar column density $N_{\rm H} \approx 1 \times 10^{20}$ cm^{-2} and an emitting area with $R^{\infty} \approx 17$ km (assuming a distance to RX J1856.5–3754 of 140 pc), temperature $T^{\infty} \approx 4.3 \times 10^5$ K, gravitational redshift $z_g \sim 0.22$, atmospheric hydrogen column $y_{\rm H} \approx 1$ g cm^{-2}, and magnetic field $B \approx (3\text{–}4) \times 10^{12}$ G; the values for the temperature and magnetic field indicate an effective average over the surface.

W.C.G. Ho (✉) · D.L. Kaplan
Kavli Institute for Astrophysics and Space Research,
Massachusetts Institute of Technology, Cambridge,
MA 02139, USA
e-mail: wynnho@slac.stanford.edu

P. Chang
Department of Astronomy, University of California,
601 Campbell Hall, Berkeley, CA 94720, USA

M. van Adelsberg
Center for Radiophysics and Space Research,
Department of Astronomy, Cornell University, Ithaca,
NY 14853, USA

A.Y. Potekhin
Ioffe Physico-Technical Institute, Politekhnicheskaya 26,
194021 St Petersburg, Russia

Keywords Stars: atmospheres · Stars: individual (RX J1856.5–3754) · Stars: neutron · X-rays: stars

PACS 97.60.Jd · 97.10.Ex

1 Introduction

Seven candidate isolated, cooling neutron stars (INSs) have been identified by the ROSAT All-Sky Survey, of which the two brightest are RX J1856.5–3754 and RX J0720.4–3125 (see Treves et al. 2000; Pavlov et al. 2002; Kaspi et al. 2006 for a review). These objects share the following properties: (1) high X-ray to optical flux ratios of $\log(f_{\rm X}/f_{\rm optical}) \sim 4\text{–}5.5$, (2) soft X-ray spectra that are well described by blackbodies with $kT \sim 50\text{–}100$ eV, (3) relatively steady X-ray flux over long timescales, and (4) lack of radio pulsations.

For the particular INS RX J1856.5–3754, single temperature blackbody fits to the X-ray spectra underpredict the optical flux by a factor of ∼6–7 (see Fig. 5). X-ray and optical/UV data can best be fit by two-temperature blackbody models with $kT_{\rm X}^{\infty} = 63$ eV, emission size $R_{\rm X}^{\infty} = 5.1\,(d/140\,{\rm pc})$ km,[1] $kT_{\rm opt}^{\infty} = 26$ eV, and $R_{\rm opt}^{\infty} = 21.2\,(d/140\,{\rm pc})$ km (Burwitz et al. 2001, 2003; van Kerkwijk and Kulkarni 2001a; Braje and Romani 2002; Drake et al. 2002; Pons et al. 2002; see also Pavlov et al. 2002;

[1] The most recent determination of the distance to RX J1856.5–3754 is ≈160 pc (Kaplan et al., in preparation). However, the uncertainties in this determination are still being examined. Therefore, we continue to use the previous estimate of 140(±40) pc from Kaplan et al. (2002) since the uncertainty in this previous value encompasses both the alternative estimate of 120 pc from Walter and Lattimer (2002) and the new value.

Trümper et al. 2004), where $T^{\infty} = T_{\rm eff}/(1+z_g)$, $R^{\infty} = R^{\rm em}(1+z_g)$, and $R^{\rm em}$ is the physical size of the emission region. The gravitational redshift z_g is given by $(1+z_g) = (1-2GM/Rc^2)^{-1/2}$, where M and R are the mass and radius of the NS, respectively. However, the lack of X-ray pulsations (down to the 1.3% level) puts severe constraints on such two-temperature models (Drake et al. 2002; Ransom et al. 2002; Burwitz et al. 2003). It is possible that the magnetic axis is aligned with the spin axis or the hot magnetic pole does not cross our line of sight (Braje and Romani 2002). Alternatively, RX J1856.5–3754 may possess a superstrong magnetic field ($B \gtrsim 10^{14}$ G) and has spun down to a period $>10^4$ s (Mori and Ruderman 2003), though Toropina et al. (2006) argue that this last case cannot explain the Hα nebula found around RX J1856.5–3754 (van Kerkwijk and Kulkarni 2001b). On the other hand, a single uniform temperature is possible if the field is not dipolar but small-scale (perhaps due to turbulence at the birth of the NS; see, e.g., Bonanno et al. 2005, and references therein).

Even though blackbody spectra fit the data, one expects NSs to possess atmospheres of either heavy elements (due to debris from the progenitor) or light elements (due to gravitational settling or accretion); we note that a magnetized hydrogen atmosphere may provide a consistent explanation for the broad spectral feature seen in the atmosphere of RX J0720.4–3125 (Haberl et al. 2004; Kaplan and van Kerkwijk 2005). The lack of any significant spectral features in the X-ray spectrum argues against a heavy element atmosphere (Burwitz et al. 2001, 2003), whereas single temperature hydrogen atmosphere fits overpredict the optical flux by a factor of ∼100 (Pavlov et al. 1996; Pons et al. 2002; Burwitz et al. 2003). However, these hydrogen atmosphere results are derived using non-magnetic atmosphere models. Only a few magnetic (fully ionized) hydrogen or iron atmospheres have been considered (e.g., Burwitz et al. 2001, 2003), and even these models are not adequate. Since $kT \sim$ tens of eV for RX J1856.5–3754 and the ionization energy of hydrogen at $B = 10^{12}$ G is 160 eV, the presence of neutral atoms must be accounted for in the magnetic hydrogen atmosphere models; the opacities are sufficiently different from the fully ionized opacities that they can change the atmosphere structure and continuum flux (Ho et al. 2003; Potekhin et al. 2004), which can affect fitting of the observed spectra.

Another complication in fitting the observational data of RX J1856.5–3754 (and RX J0720.4–3125) with hydrogen atmosphere models is that the model spectra are harder at high X-ray energies. On the other hand, observations of RX J0720.4−3125 suggest it possesses a dipole magnetic field $B \approx 2\times10^{13}$ G (Kaplan and van Kerkwijk 2005). It is probable then that RX J0720.4−3125 (and possibly RX J1856.5–3754) is strongly magnetized with $B \sim 10^{13}$–10^{14} G, and its high energy emission is softened by the effect of vacuum polarization, which can show steeper high energy tails (Ho and Lai 2003). Rather than resorting to a superstrong magnetic field, an alternate possibility is that there exists a "suppression" of the high energy emission. One such mechanism is examined in Motch et al. (2003; see also Zane et al. 2004), specifically, a geometrically thin hydrogen atmosphere at the surface that is optically thick to low energy photons and optically thin to high energy photons. The high energy photons that emerge then bear the signature of the lower temperature (compared to atmospheres that are optically thick at all energies) at the inner boundary layer (usually taken to be a blackbody) of the atmosphere model; this leads to a softer high energy tail. Motch et al. (2003) find a good fit to RX J0720.4–3125 in this case by using a non-magnetic atmosphere model with $kT_{\rm eff} = 57$ eV, a hydrogen column density $y_{\rm H} = 0.16$ g cm^{-2}, and distance of 204 pc, and assuming a $M = 1.4M_{\odot}$, $R = 10$ km NS.

We examine this last possibility by fitting the entire spectrum of RX J1856.5–3754 with the latest partially ionized hydrogen atmosphere models (constructed using the opacity and equation of state tables from Potekhin and Chabrier 2003) and condensed matter in strong magnetic fields (see van Adelsberg et al. 2005). The goal of the paper is to provide a self-consistent picture of RX J1856.5–3754 that resolves the major observational and theoretical inconsistencies: (1) blackbodies fit the spectrum much better than realistic atmosphere models, (2) strong upper limits on X-ray pulsations suggest RX J1856.5–3754 may have a largely uniform temperature (and hence magnetic field) over the entire NS surface, (3) the inferred emission size from blackbody fits are either much smaller or much larger than the canonical NS radius of 10–12 km. Because of observational uncertainties (see Sect. 3) and the computationally tedious task of constructing a complete grid of models, we do not attempt to prove the uniqueness of our results; rather we try only to reproduce the overall spectral energy distribution and argue for the plausibility of our model.

2 Models of neutron star atmospheres

Thermal radiation from a NS is mediated by the atmosphere (with scaleheight ∼1 cm). In the presence of magnetic fields typical of INSs ($B \gtrsim 10^{12}$ G), radiation propagates in two polarization modes (see, e.g., Mészáros 1992). Therefore, to determine the emission properties of a magnetic atmosphere, the radiative transfer equations for the two coupled photon polarization modes are solved (see Ho et al. 2003; Potekhin et al. 2004, and references therein for details on the construction of the atmosphere models). We note that the atmosphere models formally have a dependence, through hydrostatic balance, on the surface gravity g $[= (1+z_g)GM/R^2]$ and thus the NS radius R; however,

the emergent spectra do not vary much using different values of g around 2×10^{14} cm s^{-2} (Pavlov et al. 1995). Nevertheless, we construct models using a surface gravity that is consistent with the inferred radius obtained from the spectral fits in Sect. 4 ($g = 1.1 \times 10^{14}$ cm s^{-2} with $M = 1.4 M_\odot$, $R = 14$ km, and $z_g = 0.2$). Also, though our atmosphere models can have a magnetic field at an arbitrary angle Θ_B relative to the surface normal, the models considered here have the magnetic field aligned perpendicular to the stellar surface. Since the magnetic field and temperature distributions over the NS surface are unknown, synthetic spectra from the whole surface are necessarily model-dependent. However, if the temperature variation is large (so that a small surface area emits at high $T_{\rm eff}$ and a large area emits at lower $T_{\rm eff}$) and because spectra for various Θ_B can be qualitatively similar (see, e.g., Zavlin et al. 1995; Lloyd 2003), then a single magnetic field and temperature model can approximately describe the overall spectrum (see Ho et al. 2007 for more detailed calculations, including surface B and T variations). We describe other elements of our atmosphere models below.

2.1 Partially ionized atmospheres

As discussed in Sect. 1, previous works that attempted to fit the spectra of RX J1856.5–3754 and other INSs with magnetic hydrogen atmosphere models assume the hydrogen is fully ionized. The temperature obtained using these models (or simple blackbodies) are in the range $kT^\infty \approx 40 - 110$ eV. Contrast this with the atomic hydrogen binding energies of 160 eV and 310 eV at $B = 10^{12}$ G and 10^{13} G, respectively. Therefore the atmospheric plasma must be partially ionized.

Figure 1 illustrates the spectral differences between a fully ionized and a partially ionized hydrogen atmosphere. The atomic fraction is <10% throughout the atmosphere, where the atomic fraction is the number of H atoms with non-destroyed energy levels divided by the total number of protons (see Potekhin and Chabrier 2003; Ho et al. 2003). Besides the proton cyclotron line at $\lambda_{Bp} = 1966 (B/10^{12}\ {\rm G})^{-1} (1 + z_g)$ Å, the other features are due to bound-bound and bound-free transitions. In particular, these are the $s = 0$ to $s = 1$ transition at (redshifted) wavelength $\lambda = 170$ Å, the $s = 0$ to $s = 2$ transition at $\lambda = 110$ Å, and the bound-free transition at $\lambda = 61$ Å. The quantum number s measures the B-projection of the relative proton-to-electron angular momentum (see, e.g., Lai 2001). For a moving atom, this projection is not an integral of motion, but nonetheless the quantum number s (or $m = -s$) remains unambiguous and convenient for numbering discrete states of the atom (see Potekhin 1994). Because of magnetic broadening, the features resemble dips rather than ordinary spectral lines (see Ho et al. 2003).

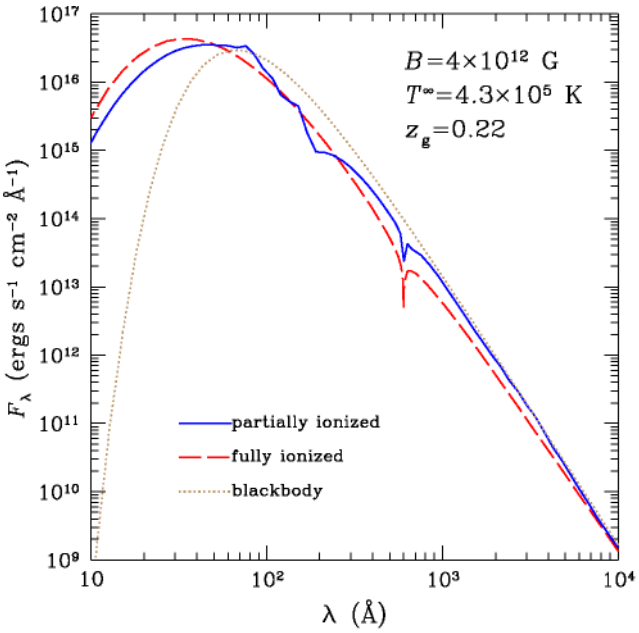

Fig. 1 Spectra of hydrogen atmospheres with $B = 4 \times 10^{12}$ G and $T^\infty = 4.3 \times 10^5$ K. The *solid line* is for a partially ionized atmosphere, the *dashed line* is for a fully ionized atmosphere, and the *dotted line* is for a blackbody. All spectra are redshifted by $z_g = 0.22$

2.2 Thin atmospheres

Conventional NS atmosphere models assume the atmosphere is geometrically thick enough so that it is optically thick at all photon energies (optical depth $\tau_\lambda \gg 1$ for all wavelengths λ); thus the observed photons are all created within the atmosphere layer. The input spectrum (usually taken to be a blackbody) at the bottom of the atmosphere is not particularly important in determining the spectrum seen above the atmosphere since photons produced at this innermost layer undergo many absorptions/emissions. The observed spectrum is determined by the temperature profile and opacities of the atmosphere. For example, atmosphere spectra are harder than a blackbody (at the same temperature) at high energies as a result of the non-grey opacities (see Fig. 1); the opacities decline with energy so that high energy photons emerge from deeper, hotter layers in the atmosphere than low energy photons.

On the other hand, consider an atmosphere that is geometrically thinner than described above, such that the atmosphere is optically thin at high energies but is still optically thick at low energies ($\tau_\lambda < 1$ for $\lambda < \lambda_{\rm thin}$ and $\tau_\lambda > 1$ for $\lambda > \lambda_{\rm thin}$). Thus photons with wavelength $\lambda < \lambda_{\rm thin}$ pass through the atmosphere without much attenuation (and their contribution to thermal balance is small since most of the energy is emitted at $\lambda > \lambda_{\rm thin}$ in the case of RX J1856.5–3754). This is illustrated in Fig. 2. Thus if the innermost atmosphere layer (at temperature $T_{\rm thin}$) emits as a black-

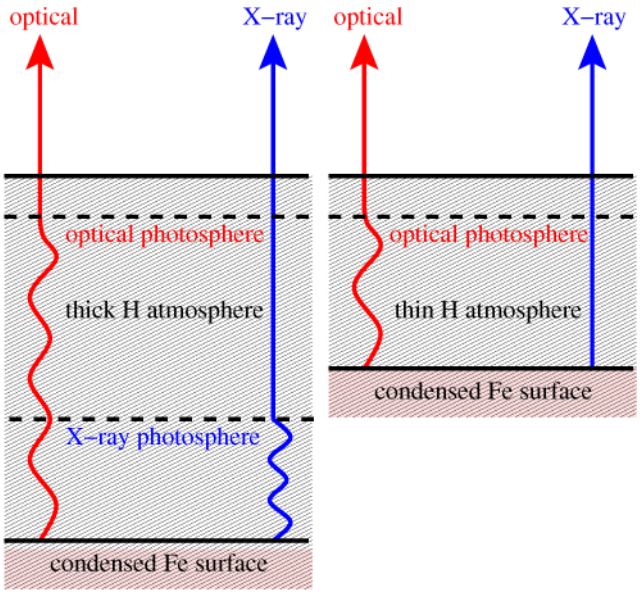

Fig. 2 Schematic diagram illustrating the difference between a "thick" atmosphere (*left*) that is optically thick to photons of all wavelengths versus a "thin" atmosphere (*right*) that is optically thick to long wavelength photons but optically thin to short wavelength photons

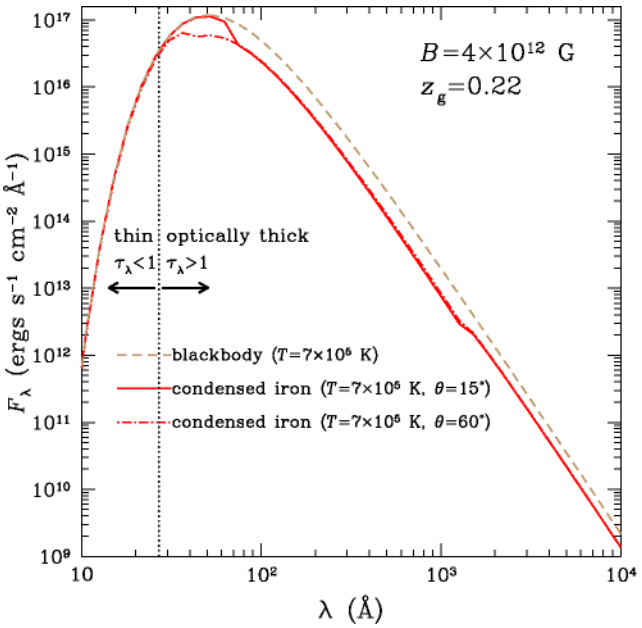

Fig. 3 Condensed iron spectrum (*solid line* for photon propagation direction $\theta = 15°$ and *dot-dashed* line for $\theta = 60°$) with $B = 4 \times 10^{12}$ G, $T = 7 \times 10^5$ K, and $\rho = 2.35 \times 10^4$ g cm^{-3}, compared to a blackbody (*dashed line*) with the same temperature. All spectra are redshifted by $z_g = 0.22$. The *vertical line* separates the wavelength ranges where the atmosphere is optically thin ($\tau_\lambda < 1$) and optically thick ($\tau_\lambda > 1$)

body, then the observed spectrum at $\lambda < \lambda_{\rm thin}$ will just be a blackbody spectrum at temperature $T = T_{\rm thin}$. Motch et al. (2003) showed that a "thin" atmosphere can yield a softer high energy spectrum than a "thick" atmosphere and used a thin atmosphere spectrum to fit the observations of RX J0720.4−3125. How such thin hydrogen atmospheres may be created is discussed in Ho et al. (2007).

2.3 Condensed iron versus blackbody emission

In addition to atmosphere models in which the deepest layer of the atmosphere is assumed to be a blackbody, we construct (more realistic and self-consistent) models in which this layer undergoes a transition from a gaseous atmosphere to a condensed surface. A surface composed of iron is a likely end-product of NS formation, and Fe condenses at $\rho \approx 561\, AZ^{-3/5} B_{12}^{6/5}$ g cm^{-3} $\approx 2.35 \times 10^4$ g cm^{-3} and $T \lesssim 10^{5.5} B_{12}^{2/5}$ K $\approx 5.5 \times 10^5$ K for the case considered here (Lai 2001); note that there is several tens of percent uncertainty in the condensation temperature (Medin and Lai, private communication; see also Medin and Lai 2006a, 2006b). Hydrogen condenses at $T \sim 2 \times 10^4 B_{12}^{0.65}$ K and thus requires much lower temperatures than is relevant for our case. The condensed matter surface possesses different emission properties than a pure blackbody (Brinkmann 1980; Turolla et al. 2004; van Adelsberg et al. 2005; Pérez-Azorín et al. 2005); in particular, features can appear at the plasma and proton cyclotron frequencies.[2]

We use the calculations of van Adelsberg et al. (2005) to determine the input spectrum in our radiative transfer calculations of the atmosphere. However, at the temperature ($T_{\rm thin} \approx 7 \times 10^5$ K) of the condensed layer relevant to our thin atmosphere models that fit the spectrum of RX J1856.5–3754, the input spectrum (where $\tau_\lambda \lesssim 1$) is effectively unchanged from a blackbody (since the temperature profile is nearly identical, with $\Delta T_{\rm thin} \sim 3\%$). Thus there are only slight differences in the resulting surface spectrum. This is illustrated in Fig. 3, where we show the emission spectrum from a $B = 4 \times 10^{12}$ G condensed iron surface at $T = 7 \times 10^5$ K and $\rho = 2.35 \times 10^4$ g cm^{-3} and compare this to a blackbody at the same temperature. The deviation from a blackbody is smaller at low angles of photon propagation θ and increases for increasing θ, as illustrated by the two angles $\theta = 15°$ and 60° (see van Adelsberg et al. 2005). Thus for most angles θ, the condensed surface spectra at short

[2] van Adelsberg et al. (2005) consider an approximation in their treatment of the ion contribution to the dielectric tensor which leads to a spectral feature at the proton cyclotron frequency. However, because of the uncertainty in this approximation, the strength of the feature is not well-determined. Nevertheless, our results are not at all strongly dependent on this feature (or the input spectrum at these low energies) because the optical depth of the atmosphere $\tau_\lambda \gg 1$ at the proton cyclotron (and plasma) frequency (see text for discussion).

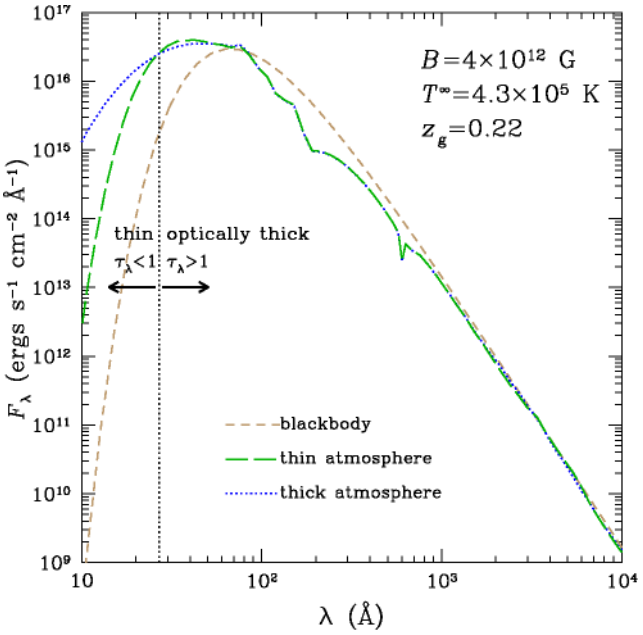

Fig. 4 Spectra of hydrogen atmospheres with $B = 4 \times 10^{12}$ G and $T^{\infty} = 4.3 \times 10^5$ K. The *dotted* and *long-dashed lines* are the model spectra using the "thick" atmosphere and "thin" atmosphere with $y_{\rm H} = 1.2$ g cm^{-2}, respectively (see text for details). The *short-dashed* line is for a blackbody with the same temperature. All spectra are redshifted by $z_g = 0.22$. The *vertical line* separates the wavelength ranges where the atmosphere is optically thin ($\tau_\lambda < 1$) and optically thick ($\tau_\lambda > 1$)

wavelengths (where $\tau_\lambda \ll 1$, so that this surface is visible to an observer above the atmosphere) are virtually identical to a blackbody. On the other hand, the atmosphere is optically thick at longer wavelengths, where the condensed surface spectra deviate from a blackbody; thus the condensed surface and the spectral features are not visible. The resulting atmosphere spectra seen by a distant observer are shown in Fig. 4. The harder spectrum at high energies in the "thick" atmosphere becomes much softer in the "thin" atmosphere and takes on a blackbody shape. In contrast, there is a negligible difference where the atmosphere is optically thick.

3 Observations and analysis

We collect publically available optical, UV, and X-ray data on RX J1856.5–3754. These data have been discussed elsewhere so our treatment will be brief. First, we assemble the optical (B- and R-band) photometry from the Very Large Telescope (VLT) from van Kerkwijk and Kulkarni (2001a) and the *Hubble Space Telescope* (*HST*) WFPC2 F170W, F300W, F450W, and F606W photometry (Walter 2001; Pons et al. 2002) as analyzed by van Kerkwijk and Kulkarni (2001a). We also take the optical VLT spectrum from van Kerkwijk and Kulkarni (2001a) and a STIS far-UV spectrum.[3] The spectra are entirely consistent with the photometry as calibrated by van Kerkwijk and Kulkarni (2001a), although given the limited signal-to-noise ratio of the spectra, we rely primarily on the photometry in what follows. We then use the *Extreme Ultraviolet Explorer* (*EUVE*; Haisch et al. 1993) data as discussed and reduced by Pons et al. (2002). Finally, we take the RGS spectrum from the 57-ks *XMM-Newton* observation and the 505-ks *Chandra* LETG spectrum that are discussed by Burwitz et al. (2003).

A source of uncertainty is that, as mentioned by Burwitz et al. (2003), the RGS and LETG data are not entirely consistent in terms of flux calibration: while they have very similar shapes (and hence implied temperatures and absorptions) the radii inferred from blackbody fits differ by as much as 10% and the overall flux by as much as 20%. Since the LETG fits in Burwitz et al. (2003) are more consistent with those of the CCD instruments on *XMM-Newton* (EPIC-pn and EPIC-MOS2) and in our opinion the current low-energy calibration of LETG is more reliable, we adjust the flux of the RGS data upward by 17% to force agreement with the *Chandra* data. We do not know for certain which calibration (if either) is entirely accurate, so some care must be taken when interpreting the results at the 10–20% level. Fully reliable calibration or even cross-calibration at the low-energy ends of the *Chandra* and *XMM-Newton* responses (<0.2 keV) is not currently available (see, e.g., Kargaltsev et al. 2005), and the detailed response of *EUVE* compared to those of *Chandra* and *XMM-Newton* is also unknown. Therefore, for accuracy in doing the EUV/X-ray fits, we concentrate on the LETG data, which are consistent and have high-quality calibration.

We follow the HRC-S/LETG analysis threads "Obtain Grating Spectra from LETG/HRC-S Data,"[4] "Creating Higher-order Responses for HRC-S/LETG Spectra,"[5] "Create Grating RMFs for HRC Observations,"[6] and "Compute LETG/HRC-S Grating ARFs"[7] and use CIAO[8] version 3.2.2 and CALDB version 3.2.2. We extracted the dispersed events and generated response files for orders ±1, ±2, and ±3. After fitting the LETG data, we compare the fit results qualitatively with the RGS and *EUVE* data; the general agreement is good, but we do not use them quantitatively.

[3] Datasets: O5G702010-O5G702050, O5G703010-O5G703050, O5G704010-O5G704050, O5G705010-O5G705050, O5G751010-O5G751050, O5G752010-O5G752050. O5G701010-O5G701050, and

[4] See http://asc.harvard.edu/ciao/threads/spectra_letghrcs/.

[5] See http://asc.harvard.edu/ciao/threads/hrcsletg_orders/.

[6] See http://asc.harvard.edu/ciao/threads/mkgrmf_hrcs/.

[7] See http://asc.harvard.edu/ciao/threads/mkgarf_letghrcs/.

[8] http://cxc.harvard.edu/ciao/.

Table 1 Fits to the X-ray data. Numbers in parentheses are 68% confidence limits in the last digit(s). The formal fit uncertainty for $R^{\infty} < 10\%$; however, since the radius determination depends on the distance, we conservatively adopt the current ∼30% distance uncertainty as our radius uncertainty

	Atmosphere	Blackbody
	Model parameters	
B (10^{12} G)	4	
$y_{\rm H}$ (g cm^{-2})	1.2	
	Fit results	
$N_{\rm H}$ (10^{20} cm^{-2})	1.30(2)	0.91(1)
T^{∞} (10^5 K)	4.34(2)	7.36(1)
R^{∞} (d_{140} km)	17	5.0
z_g	0.22(2)	
$\chi^2_{\rm r}$/dof	0.86/4268	0.86/4269

4 Atmosphere model fitting

Because of data reduction and cross-calibration issues (see Sect. 3) and possible variations in the interstellar absorption abundances (standard abundances are assumed), we do not feel that a full fit of the data is justified at this time. Therefore we do not fit for all of the parameters in a proper sense nor do we perform a rigorous search of parameter space. Instead, we fit for a limited subset of parameters while varying others manually. This allows us to control the fits in detail and reduce the computational burden of preparing a continuous distribution (in B, $T_{\rm eff}$, and $y_{\rm H}$) of models, yet still determine whether our model qualitatively fits the data.

For a given magnetic field and atmosphere thickness, we generate partially ionized atmosphere models for a range of effective temperatures. (Note that, since the continuum opacity of the dominant photon polarization mode decreases for increasing magnetic fields, the required thickness $y_{\rm H}$ of the atmosphere increases for increasing B.) We then perform a χ^2 fit in `CIAO` to the LETG data over the 10–100 Å range (0.12–1.2 keV) for the absorption column density $N_{\rm H}$ [using the `TBabs` absorption model from `Xspec` (Wilms et al. 2000), although other models such as `phabs` give similar results], the temperature T^{∞}, the normalization (parameterized by R^{∞}), and the redshift z_g, where we interpolate over T^{∞}. We obtain a good fit, and Table 1 lists the best-fit parameters and model; the radius is given assuming a distance $d_{140} = d/(140\ {\rm pc}) = 1$ (see footnote 1). While we find a range of magnetic fields [$B \approx (3{-}4) \times 10^{12}$ G] that give acceptable fits, changes in the magnetic field outside this range (but still within $B = 10^{12}{-}10^{13}$ G) and atmosphere thickness lead to worse fits. At $B > 10^{13}$ G, spectral features due to proton cyclotron and bound species appear in the observable soft X-ray range (though they are likely to be broadened due to magnetic field variations over the surface of the NS), which are not seen.

To further evaluate the quality of this fit, we fit the same LETG data with a blackbody. The blackbody fit yields parameters (see Table 1) that are very similar to those derived by Burwitz et al. (2003; see Sect. 1). Given the comparable $\chi^2_{\rm r}$ (≈1) we achieve from our blackbody and atmosphere model fits (along with the low-energy calibration uncertainties), we are confident that the atmosphere model describes the observations just as well as a blackbody.

Next, we examine the quality of the fit to the optical/UV data. van Kerkwijk and Kulkarni (2001a) showed that these data are well fit by a Rayleigh–Jeans power law ($F_\lambda \propto \lambda^{-4}$) with an extinction $A_V = 0.12 \pm 0.05$ mag. In our fitting, we try using both the optical extinction implied by the X-ray absorption ($A_V = N_{\rm H}/(1.79 \times 10^{21}\ {\rm cm}^{-2})$ mag; Predehl and Schmitt 1995) and fitting freely for A_V, but we find that these fits are too unconstrained and that the value of A_V is not sensitively determined by the data (indeed, this is reflected in the large uncertainties found by van Kerkwijk and Kulkarni 2001a). As a result, we fix A_V to 0.12 mag. We also assume a single value for the reddening ($R_V = 3.1$) and use the reddening model of Cardelli et al. (1989) with corrections from O'Donnell (1994). We find that our best-fit model to the X-ray data also produces a λ^{-4} power law but underpredicts the optical/UV data by a factor of 15–20%.[9] Looking in detail at the highest quality optical data point (the *HST* F606W measurement), we find that it is 15% above our model spectra. However, the error budget is 3% (photometric uncertainty), 5% (A_V uncertainty), 10% (uncertainty in the optical model flux), and 5% (uncertainty in the fitted optical flux due to the X-ray normalization), and therefore the 15% disagreement can easily be explained by known sources of uncertainty.

Figure 5 shows the observations of RX J1856.5–3754. We also overlay the blackbody and our $B = 4 \times 10^{12}$ G atmosphere model spectra with the parameters given in Table 1. As discussed in Sect. 1, the data are generally featureless, while the models show spectral features; at $B \approx 4 \times 10^{12}$ G, the features due to bound species lie in the extreme UV to very soft X-ray range and are thus hidden by interstellar absorption. Overall, we see that our atmosphere model spectra are generally consistent with the X-ray and optical/UV data, while a blackbody underpredicts the optical/UV by a factor of 6–7.

[9] Comparing monochromatic fluxes derived from photometry with the models is not sufficiently accurate for a detailed, quantitative analysis. A more accurate method would involve convolving the models with the filter bandpasses and predicting monochromatic count-rates to compare with the data (e.g., van Kerkwijk and Kulkarni 2001a; Kaplan et al. 2003). However, given the assumptions about extinction and reddening and the level of accuracy of this analysis, the first approach will suffice here.

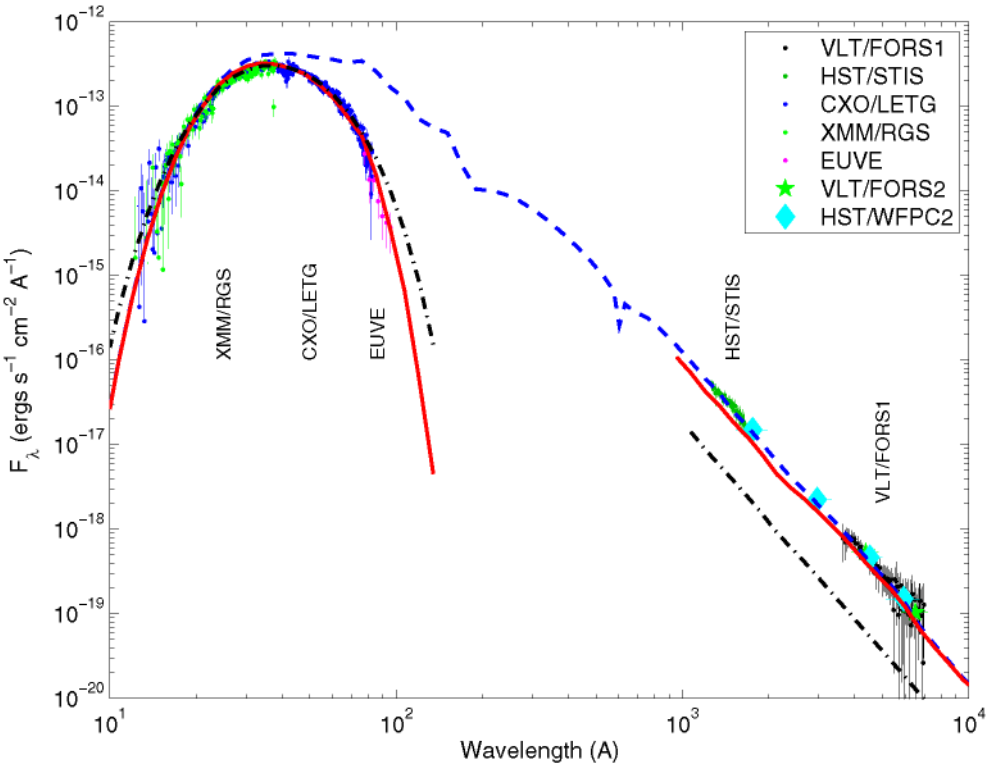

Fig. 5 Spectrum of RX J1856.5–3754 from optical to X-ray wavelengths. The data points are observations taken from various sources. Error bars are one-sigma uncertainties. Optical spectra are binned for clarity: STIS data into 30 bins at a resolution of 12 Å and VLT data into 60 bins at 55 Å resolution. The *solid line* is the absorbed (and redshifted by $z_g = 0.22$) atmosphere model spectrum with $B = 4 \times 10^{12}$ G, $y_{\rm H} = 1.2$ g cm^{-2}, $T^{\infty} = 4.3 \times 10^5$ K, and $R^{\infty} = 17$ km. The *dashed line* is the unabsorbed atmosphere model spectrum. The *dash-dotted line* is the (absorbed) blackbody fit to the X-ray spectrum with $R^{\infty} = 5$ km

5 Summary and conclusions

We have gathered together observations of the isolated neutron star RX J1856.5–3754 and compared them to our latest magnetic, partially ionized hydrogen atmosphere models. Prior works showed that the observations were well-fit by blackbody spectra. Here we obtain good fits to the overall multiwavelength spectrum of RX J1856.5–3754 using the more realistic atmosphere model. In particular, we do not overpredict the optical flux obtained by previous works and require only a single temperature atmosphere. [Note that this single temperature (and magnetic field) serves as an average value for the entire surface.] In addition to the neutron star orientation and viewing geometry, the single temperature helps to explain the non-detection of pulsations thus far. At high X-ray energies, where the atmosphere is optically thin, the model spectrum has a "blackbody-like" shape due to the emission spectrum of a magnetized, condensed surface beneath the atmosphere. The atmosphere is optically thick at lower energies; thus features in the emission spectrum of the condensed surface are not visible when viewed from above the atmosphere. The "thinness" of the atmosphere helps to produce the featureless, blackbody-like spectrum seen in the observations.

Based on a possible origin within the Upper Scorpius OB association, the age of RX J1856.5–3754 is estimated to be about 5×10^5 yr (Walter 2001; Walter and Lattimer 2002; Kaplan et al. 2002). Our surface temperature determination ($kT^{\infty} = 37$ eV) is only a factor of 1.7 below the blackbody temperature ($kT^{\infty} = 63$ eV) obtained by previous works and therefore does not place much stronger constraints on theories of neutron star cooling (see, e.g., Page et al. 2004; Yakovlev and Pethick 2004). It may also be noteworthy that RX J1856.5–3754 is one of the cooler isolated neutron stars and possibly possesses the lowest magnetic field [$B \approx (3\text{–}4) \times 10^{12}$ G]; the lower magnetic field implies a more uniform surface temperature distribution and weaker radiation beaming.

Finally, the emission radius we derive from our atmosphere model fits is $R^{\infty} \approx 17\,(d/140\,{\rm pc})$ km (although recall the distance and flux uncertainties discussed in footnote 1 and Sect. 3, respectively). Accounting for gravitational redshift ($z_g \sim 0.22$), this yields $R^{\rm em} \approx 14$ km. This is much larger than the inferred radius obtained by just fitting the X-ray data with a blackbody ($R^{\infty}_{\rm X} \approx 5$ km). As a result, there does not appear to be a need to resort to more exotic explanations such as quark or strange stars (e.g., Drake et al. 2002; Xu 2003; see Walter 2004; Weber 2005 for a review), at least for the case of RX J1856.5–3754. On the other hand, our radius is small compared to the radius derived from fitting the optical/UV data ($R^{\infty}_{\rm opt} \approx 21$ km). For a $1.4\,M_{\odot}$ neutron star, the latter implies a low redshift ($z_g \approx 0.12$) and very large intrinsic radius ($R^{\rm em}_{\rm opt} \approx 19$ km); this is ruled out by neutron star equations of state, while our radius $R^{\rm em} \approx 14$ km only requires a standard, stiff equation of state (see, e.g., Lattimer and Prakash 2001).

Acknowledgements We greatly appreciate assistance from Marten van Kerkwijk, Gilles Chabrier, Chris Thompson, Dong Lai, and Lars Bildsten. We thank the anonymous referee for useful comments. W.H. is supported by NASA through Hubble Fellowship grant HF-01161.01-A awarded by STScI, which is operated by AURA, Inc., for NASA, under contract NAS 5-26555. D.K. was partially supported by a fellowship from the Fannie and John Hertz Foundation and by HST grant GO-09364.01-A. Support for the HST grant GO-09364.01-A was provided by NASA through a grant from STScI, which is operated by AURA, Inc., under NASA contract NAS 5-26555. P.C. is supported by the NSF under PHY 99-07949, by JINA through NSF grant PHY 02-16783, and by NASA through Chandra Award Number GO4-5045C issued by CXC, which is operated by the SAO for and on behalf of NASA under contract NAS 8-03060. P.C. acknowledges support from the Miller Institute for Basic Research in Science, University of California Berkeley. A.P. is supported by FASI through grant NSh-9879.2006.2 and by RFBR through grants 05-02-16245 and 05-02-22003.

References

Bonanno, A., Urpin, V., Belvedere, G.: Astron. Astrophys. **440**, 199 (2005)
Braje, T.M., Romani, R.W.: Astrophys. J. **580**, 1043 (2002)
Brinkmann, W.: Astron. Astrophys. **82**, 352 (1980)
Burwitz, V., Zavlin, V.E., Neuhäuser, R., et al.: Astron. Astrophys. **379**, L35 (2001)
Burwitz, V., Haberl, F., Neuhäuser, R., et al.: Astron. Astrophys. **399**, 1109 (2003)
Cardelli, J.A., Clayton, G.C., Mathis, J.S.: Astrophys. J. **345**, 245 (1989)
Drake, J.J., et al.: Astrophys. J. **572**, 996 (2002)
Haberl, F., Zavlin, V.E., Trümper, J., et al.: Astron. Astrophys. **419**, 1077 (2004)
Haisch, B., Bowyer, S., Malina, R.F.: J. Br. Interplanet. Soc. **46**, 331 (1993)
Ho, W.C.G., Lai, D.: Mon. Not. Roy. Astron. Soc. **338**, 233 (2003)
Ho, W.C.G., Lai, D., Potekhin, A.Y., et al.: Astrophys. J. **599**, 1293 (2003)
Ho, W.C.G., Kaplan, D.L., Chang, P., et al.: Mon. Not. Roy. Astron. Soc. **375**, 821 (2007)
Kaplan, D.L., van Kerkwijk, M.H.: Astrophys. J. Lett. **628**, L45 (2005)
Kaplan, D.L., van Kerkwijk, M.H., Anderson, J.: Astrophys. J. **571**, 447 (2002)
Kaplan, D.L., van Kerkwijk, M.H., Marshall, H.L., et al.: Astrophys. J. **590**, 1008 (2003)
Kargaltsev, O.Y., Pavlov, G.G., Zavlin, V.E., et al.: Astrophys. J. **625**, 307 (2005)
Kaspi, V.M., Roberts, M.S.E., Harding, A.K.: In: Lewin, W.H.G., van der Klis, M. (eds.) Compact Stellar X-ray Sources. Cambridge University Press, Cambridge (2006, in press). Preprint: astro-ph/0402136
Lai, D.: Rev. Mod. Phys. **73**, 629 (2001)
Lattimer, J.M., Prakash, M.: Astrophys. J. **550**, 426 (2001)
Lloyd, D.A.: Mon. Not. Roy. Astron. Soc. (2003, submitted) (astro-ph/0303561)
Medin, Z., Lai, D.: Phys. Rev. A **74**, 062507 (2006a) (astro-ph/0607166)
Medin, Z., Lai, D.: Phys. Rev. A **74**, 062508 (2006b) (astro-ph/0607277)
Mészáros, P.: High-Energy Radiation from Magnetized Neutron Stars. University of Chicago Press, Chicago (1992)
Mori, K., Ruderman, M.A.: Astrophys. J. Lett. **592**, L75 (2003)
Motch, C., Zavlin, V.E., Haberl, F.: Astron. Astrophys. **408**, 323 (2003)
O'Donnell, J.E.: Astrophys. J. **422**, 158 (1994)
Page, D., Lattimer, J.M., Prakash, M., et al.: Astrophys. J. Suppl. Ser. **155**, 623 (2004)
Pavlov, G.G., Zavlin, V.E., Sanwal, D.: In: Becker, W., Lesch, H., Trümper, J. (eds.) Proc. 270 WE-Heraeus Seminar on Neutron Stars, Pulsars, and Supernova Remnants, p. 273. MPI, Garching (2002) (MPE Rep. 278)
Pavlov, G.G., Shibanov, Yu.A., Zavlin, V.E., Meyer, R.D.: In: Alpar, M.A., Kiziloğlu, Ü., van Paradijs, J. (eds.) Lives of the Neutron Stars, p. 71. Kluwer, Boston (1995)
Pavlov, G.G., Zavlin, V.E., Trümper, J., et al.: Astrophys. J. Lett. **472**, L33 (1996)
Pérez-Azorín, J.F., Miralles, J.A., Pons, J.A.: Astron. Astrophys. **433**, 275 (2005)
Pons, J.A., Walter, F.M., Lattimer, J.M., et al.: Astrophys. J. **564**, 981 (2002)
Potekhin, A.Y.: J. Phys. B. **27**, 1073 (1994)
Potekhin, A.Y., Chabrier, G.: Astrophys. J. **585**, 955 (2003)
Potekhin, A.Y., Lai, D., Chabrier, G., et al.: Astrophys. J. **612**, 1034 (2004)
Predehl, P., Schmitt, J.H.M.M.: Astron. Astrophys. **293**, 889 (1995)
Ransom, S.M., Gaensler, B.M., Slane, P.O.: Astrophys. J. Lett. **570**, L75 (2002)
Toropina, O.D., Romanova, M.M., Lovelace, R.V.E.: Mon. Not. Roy. Astron. Soc. **371**, 569 (2006). Preprint: astro-ph/0606254
Treves, A., Turolla, R., Zane, S., et al.: PASP **112**, 297 (2000)
Trümper, J.E., Burwitz, V., Haberl, F., et al.: Nucl. Phys. B Proc. Suppl. **132**, 560 (2004)
Turolla, R., Zane, S., Drake, J.J.: Astrophys. J. **603**, 265 (2004)
van Adelsberg, M., Lai, D., Potekhin, A.Y., et al.: Astrophys. J. **628**, 902 (2005)
van Kerkwijk, M.H., Kulkarni, S.R.: Astron. Astrophys. **378**, 986 (2001a)
van Kerkwijk, M.H., Kulkarni, S.R.: Astron. Astrophys. **380**, 221 (2001b)
Walter, F.M.: Astrophys. J. **549**, 433 (2001)
Walter, F.M.: J. Phys. G **30**, S461 (2004)
Walter, F.M., Lattimer, J.M.: Astrophys. J. Lett. **576**, L145 (2002)
Weber, F.: Prog. Part. Nucl. Phys. **54**, 193 (2005)
Wilms, J., Allen, A., McCray, R.: Astrophys. J. **542**, 914 (2000)
Xu, R.X.: Astrophys. J. Lett. **596**, L59 (2003)
Yakovlev, D.G., Pethick, C.J.: Annu. Rev. Astron. Astrophys. **42**, 169 (2004)
Zane, S., Turolla, R., Drake, J.J.: Adv. Space Res. **33**, 531 (2004)
Zavlin, V.E., Pavlov, G.G., Shibanov, Yu.A., et al.: Astron. Astrophys. **297**, 441 (1995)